ARTICLES

Journal of Semiconductors
(2020) 41, 122402
doi: 10.1088/1674-4926/41/12/122402

Theoretical study of a group IV p–i–n photodetector with a flat and broad response for visible and infrared detection

Jinyong Wu[1], Donglin Huang[1], Yujie Ye[1], Jianyuan Wang[1], Wei Huang[1], Cheng Li[1], Songyan Chen[1, †], and Shaoying Ke[2, †]

[1]Key Laboratory of Low Dimensional Condensed Matter Physics (Department of Education of Fujian Province), Collaborative Innovation Center for Optoelectronic Semiconductors and Efficient Devices, Department of Physics, Xiamen University, Xiamen 361005, China

[2]College of Physics and Information Engineering, Minnan Normal University, Zhangzhou 363000, China

Abstract: We report a theoretical study of a broadband Si/graded-SiGe/Ge/$Ge_{0.9}Sn_{0.1}$ p–i–n photodetector with a flat response based on modulating thickness of the layers in the active region. The responsivity of the photodetector is about 0.57 A/W in the range of 700 to 1800 nm. This structure is suitable for silicon-based epitaxial growth. Annealing is technically applied to form the graded-SiGe. The photodetector reaches a cut-off wavelength at ~2300 nm and a low dark-current density under 3 V reverse bias about 0.17 mA/cm^2 is achieved theoretical at room temperature. This work is of great significance for silicon-based detection and communication, from visible to infrared.

Key words: flat response; broad response; dark current density; graded-SiGe; $Ge_{0.9}Sn_{0.1}$

Citation: J Y Wu, D L Huang, Y J Ye, J Y Wang, W Huang, C Li, S Y Chen, and S Y Ke, Theoretical study of a group IV p–i–n photodetector with a flat and broad response for visible and infrared detection[J]. *J. Semicond.*, 2020, 41(12), 122402. http://doi.org/10.1088/1674-4926/41/12/122402

1. Introduction

In the last few decades, broad spectral response photodetectors have drawn substantial attention due to their potential applications. A broadband photodetector can detect from visible (Vis) to infrared (IR) light. The range covers all telecommunication bands. This is particularly important in the commercial applications of imaging sensors, civil engineering, telecommunications, biomedicine, environmental monitoring, and defence sensing[1–4].

To obtain broadband detection, many efforts have been made to fabricate broadband photodetectors in recent years. For example, Qiao *et al.*[5] reported a graphene/Bi_2Te_3 photodetector with a broadband response from 532 to 1550 nm, the photocurrent ranges from 0.2 to 1.7 μA at an optical power of 1.28 μW. Yuan *et al.*[6] demonstrated a broadband photodetector using a laminated black phosphorus transistor that is polarization-sensitive over a range from 400 to 3750 nm, whereas the response of this detector is relatively low. Hu *et al.*[7] designed and fabricated a Ge/perovskite broadband photodetector. The detector shows excellent responsivity of 228 and 1.4 A/W at 680 and 1550 nm, respectively. However, the responsivity of these detectors varies greatly under optical signals of different wavelengths. This is not conducive to the selection of amplifiers in subsequent circuits. These devices are not compatible with Si complementary metal oxide semiconductor (CMOS) processing technology, which greatly limits their commercial application.

In the mature group IV materials, Si photodetectors are suitable for the detection of Vis range. Ge has favorable optoelectronic properties at the NIR range, whereas the response of the Ge photodetector at 1550 nm (telecommunication band) is typically drastically reduced. Therefore, the Si and Ge photodetectors are not suitable for the broadband detection. As a new IV group alloy, germanium–tin alloy (GeSn) has recently attracted significant research interest due to its tunable bandgap[8, 9]. The increase of Sn content in GeSn leads to a decrease of bandgap. This results in the extension of detection range of GeSn photodetector[10–13]. Thus, GeSn material can be utilized in broadband detection. However, the dark current density of GeSn photodetectors is up to 0.1–1 A/cm^2[10–13]. Under optical signals of different wavelengths, the response of GeSn photodetectors also varies greatly. These factors introduce lots of noise into the detection system. Furthermore, the previous results indicate that GeSn has extremely poor response performance in the range of Vis light spectrum[13]. This is due to short Vis light penetration length in GeSn film. The photodetector based on materials with narrow bandgap suffers from dead-space effect inevitably[11]. This hinders its development in Vis-light communication and broadband detection applications.

To solve these problems, we theoretically design a structure of an entirely group IV p–i–n photodetector based on the silicon-based epitaxial growth and annealing processes. We obtained a graded-SiGe layer (The content of Ge gradually changed from 0 to 1) by performing annealing on the samples of the Ge layer grown on silicon substrate. Using graded-SiGe to enhance the absorption of Vis optical signal and $Ge_{0.9}Sn_{0.1}$ to enhance the absorption of IR optical signal, a broadband photodetector with flat response is theoretical obtained by utilizing different absorption peaks of different active layers and modulating the thickness of each layer.

Correspondence to: S Y Chen, sychen@xmu.edu.cn; S Y Ke, keshaoying2005@163.com

Received 12 MARCH 2020; Revised 28 APRIL 2020.

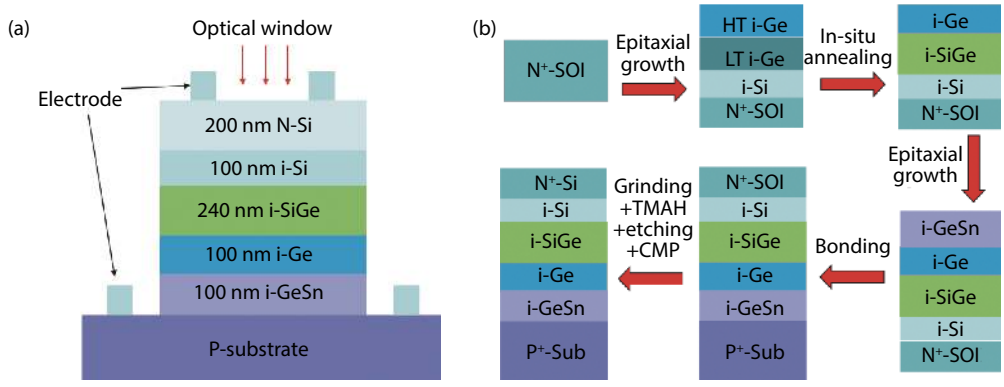

Fig. 1. (Color online) (a) Schematic cross-section of the Si/graded-SiGe/Ge/$Ge_{0.9}Sn_{0.1}$ p–i–n photodetector. The mesa size is 32 μm in diameter. (b) Schematic of epitaxial growth and layer transfer technique for this p–i–n structure fabrication.

Table 1. Parameters of Si, SiGe, Ge, and $Ge_{0.9}Sn_{0.1}$.

Material	Energy gap (eV)	Surface recombination velocity (cm/s)	Threading dislocation density (TDD) (cm^{-2})	*n*, *k*
Si	1.12	3.5×10^2	1×10^4	Database
SiGe	0.66–1.12	1×10^6	1×10^7[22]	Ref. [23, 24]
Ge	0.66	1×10^6	1×10^7[25]	Database
$Ge_{0.9}Sn_{0.1}$	0.495	1×10^6	1×10^7	Ref. [20]

The responsivity is about 0.57 A/W in the range of 700 to 1800 nm, which is of great help to the simplification of subsequent detection circuits and the improvement of accuracy. The photodetector reaches the cut-off f wavelength at ~2300 nm. A low dark current density under 3 V reverse bias about 0.17 mA/cm^2 is achieved after theoretical optimization at room temperature. Compared with other broadband photodetectors, due to the adjustable multi-layer structure in the active region, we can modulate the response characteristic of the detector within a certain range while obtaining a low dark current density. Therefore, this photodetector has extensive application in optical signal detection. Furthermore, the manufacturing process of the device is compatible with Si CMOS processing technology. This shows great potential for application in low cost Si-based optoelectronics[14].

2. Structure design and parameters setting

2.1. Structure design

A schematic cross-section of our device structure is presented in Fig. 1(a). We superimposed the Si/graded-SiGe/Ge/$Ge_{0.9}Sn_{0.1}$ layers on the n^+-Si substrate in the order of epitaxial growth. The graded-SiGe layer was formed by in-situ annealing (the epitaxial buffer of graded-SiGe is much thicker). The device can be prepared by bonding the epitaxial layer onto a new substrate, as shown in Fig. 1(b)[15–18]. Under the inverted structure, when the optical signal is vertically incident, the Vis optical signal is first-absorbed by Si and graded-SiGe layers. The IR optical signal continues to go deep and is mainly absorbed by Ge and $Ge_{0.9}Sn_{0.1}$ layers. We optimized the structure of the device, the bandgap of materials was linked from wide to narrow. Thus, the effect of dead-space effect is greatly alleviated. Since the absorption peaks of materials in the active region differ, we modulated the thickness of each layer to change the responsivity of different wavelength optical signals. Thereby we can modulate the spectral response, forming a flat and broad response.

2.2. Parameter setting

The Atlas simulator of the TCAD Silvaco commercial software is applied to simulate the performance of the p–i–n photodetector based on three classical equations (Poisson's equation, continuity equation, and transport equation). According to these effective theories, we can achieve the reasonable simulation data of the designed device. Here, the temperature (*T*) is set to 300 K (room temperature) when some temperature dependence equations are calculated. The responsivity (*R*) is defined as $I(g = 1)/P$, and *I* denotes the photocurrent, *g* the gain, *P* the optical power. Optical input power of incident light source is set to 0.125 W/cm^2. It is worth mentioning that there is no relevant data of GeSn in the Silvaco database. We collected the information of GeSn material, including the calculation method of bandgap[19], refractive index (*n*) and extinction coefficient (*k*) (The content of Sn is up to 10%) under optical signals of different wavelengths[20], etc. We utilize Ge as the background material to define $Ge_{0.9}Sn_{0.1}$, in addition to the parameters defined by us, other parameters of the $Ge_{0.9}Sn_{0.1}$ used in the simulation are extracted from Ge material. The main data used in the simulation are recorded in Table 1. The surface charge density of Ge material is set as 1×10^{14} cm^{-2}, and the surface recombination velocity (SRV) is 1×10^6 cm/s[21]. We use these parameters in simulation of graded-SiGe material because it is still pure Ge on its surface.

3. Simulation results

At first, we simulated the spectral response of p–i–n photodetector with single material as the active region. Meanwhile, to compare with the result of our structure as shown in Fig. 1(a), the top layer of each photodetector was set as n^+-type Si at 200 nm, both layers of p^+-type and n^+-type doping are set to be 1×10^{19} cm^{-3}. The spectral response was shown in Figs. 2(a)–2(d), respectively. The material in the p^+-substrate is consistent with that in the active region, as shown in Fig. 3(c). It is found that when the thickness of the active region in-

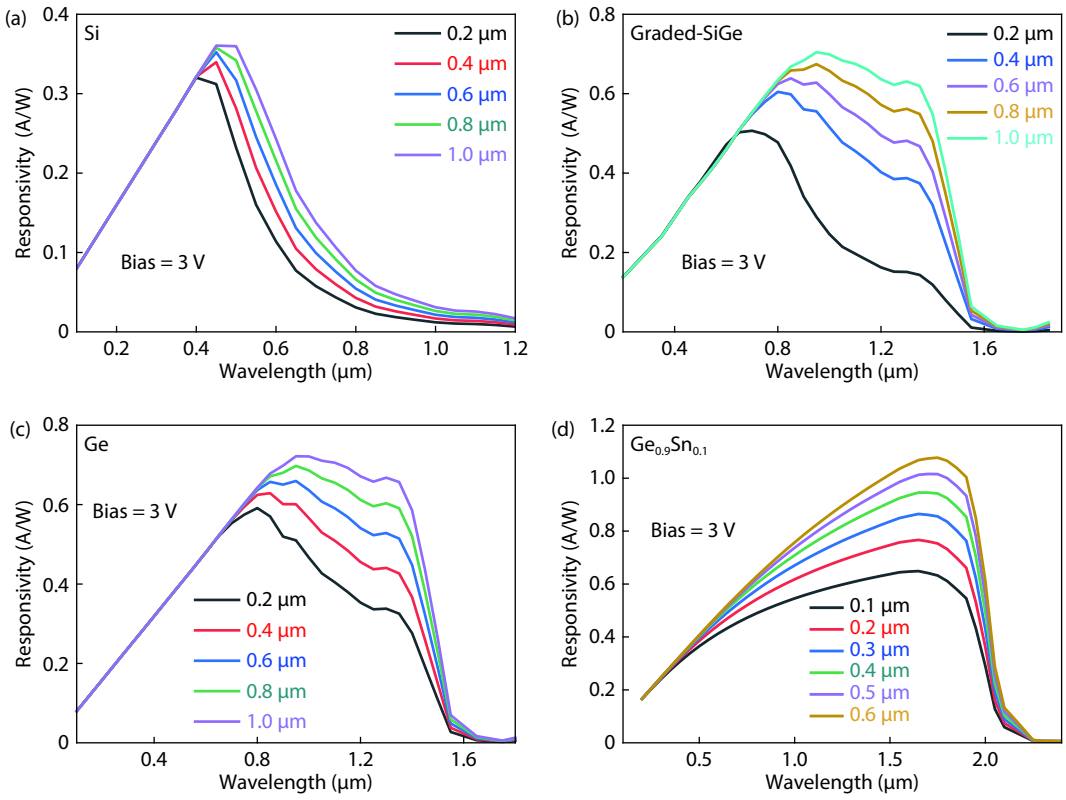

Fig. 2. (Color online) Simulation of spectral responsivity of the p–i–n photodetector with single material as active region for (a) Si, (b) graded-SiGe, (c) Ge, and (d) $Ge_{0.9}Sn_{0.1}$.

creases gradually, the peak of responsivity shows different degrees of redshift. For example, when the thickness of the active region of Si photodetector is up to several microns, the absorption peak can be redshifted to around 800 nm. However, because we use multi-layer materials to fully combine the detection ranges, the active region of the detector becomes much thicker and this results in a greatly reduced response rate. Thus, the calculation range of each active region is set within 1000 nm.

To determine the variation of Ge content in graded-SiGe, the samples of Ge epitaxial growth on Si by two-step method were annealed and performed auger electron spectroscopy (AES) characterization. The phenomenon of atomic interdiffusion appears at the interface between Si and Ge[26, 27], forming a graded-SiGe layer. Due to the changing of Ge content, the spectral response of graded-SiGe photodetector changes with the thickness of the active region. The low-temperature (LT) layer of Ge is about 100 nm, due to the high dislocation and defect density, the diffusion of Si element is mainly concentrated in the LT layer. The annealing process can minimize the dislocation in Ge layer[28] and it is beneficial to the epitaxial growth of GeSn. From Figs. 3(a) and 3(b), we find that the content of Ge in graded-SiGe rapidly increase to about 0.8 before entering the high-temperature (HT) Ge layer, and then slowly go to 1.0 in the HT Ge layer (determined by annealing conditions). Therefore, when the thickness of graded-SiGe active region is very thick, the absorption characteristic tends to be more and more similar to the characteristic of Ge, as shown in Figs. 2(b) and 2(c). With the change of thickness of absorption layer from 200 to 1000 nm, the absorption peak of Si photodetectors shifted from 400 to 500 nm. The response peak of graded-SiGe shifted from 700 to 1000 nm, and the response peak of Ge shifted from 800 to 1000 nm. The response peak of $Ge_{0.9}Sn_{0.1}$ was basically stable at 1800 nm as shown in Fig. 2(d). Note that the responsivity of longer wavelength optical signal needs a thicker active region to lead the redshift phenomenon.

There are two main sources of dark current density (J_{dark}) in the photodetector: the bulk leakage current density (J_{bulk}) and the surface leakage current density (J_{surf}). The main source of J_{surf} is the interface traps around the mesa. The interface traps can introduce energy levels in the bandgap and eventually increase the J_{surf}. Both doping and TDD have a significant effect on the minority carrier lifetime (MCL) and ultimately affect the J_{dark}. The TDD of Si material in substrate and active region is much lower than that of epitaxial Ge. The MCL of Si is mainly affected by the doping. We set the MCL of n^+-Si to 1×10^{-8} s. The MCL of Si in active region is set to 1×10^{-4} s[29]. For the MCL of Ge film in active region, the effect of TDD cannot be ignored. We set the MCL of Ge material to 5×10^{-5} s[30]. The MCLs of SiGe and GeSn are consistent with that of Ge material. To take into account the effect of surface recombination, we compared the effect of SRV on the J_{dark}. It is observed in Fig. 3(d) that the effect on the J_{dark} is not significant when the SRV is 1×10^6 cm/s or below, and the J_{dark} begin to increase when the SRV is higher than this order. Therefore, under such settings, the contribution of J_{bulk} to J_{dark} is more significant. Different from the simulation of spectral response, considering that J_{surf} varies from different materials, in the simulation of J_{dark}, the p^+-region, i-region and n^+-region of each photodetector is set as the same material. The J_{dark} of the p–i–n photodetector with singlesingle material and $Ge_{0.9}Sn_{0.1}$, as shown in Figs. 4(a)–4(d), respectively. We used relatively ideal materials for the simulation, the J_{dark} is

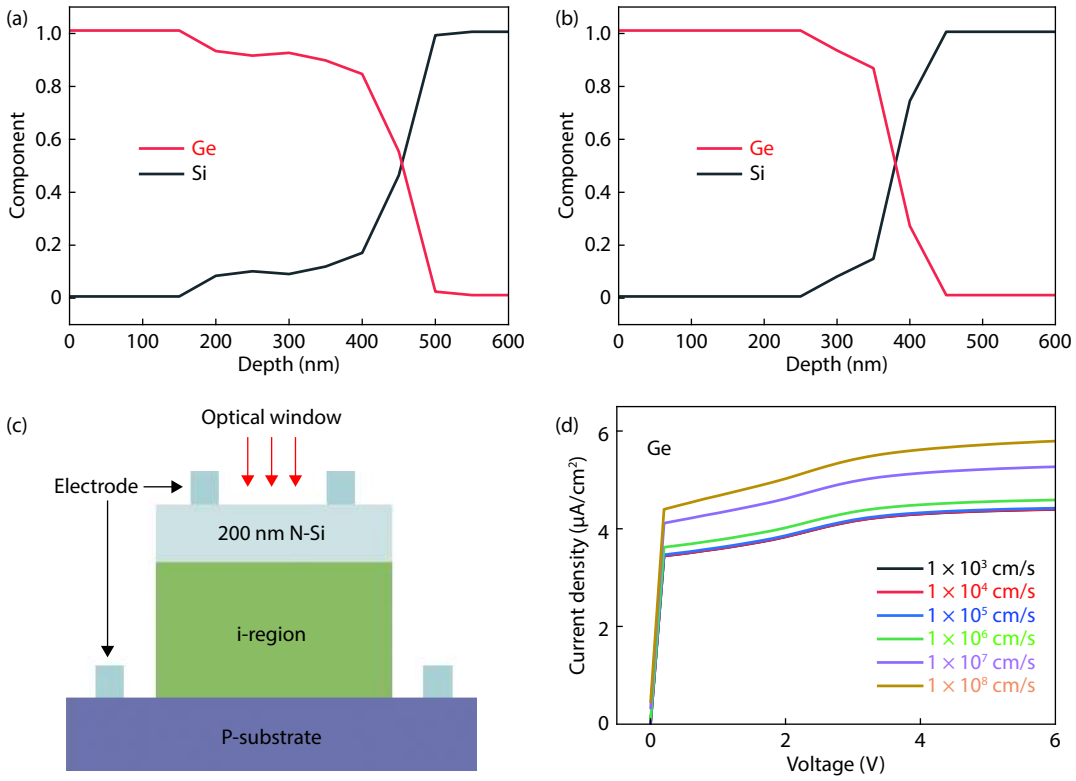

Fig. 3. (Color online) (a) AES of the sample annealed at 800 °C for 30 min and 900 °C for 0 s. (b) AES of the sample annealed at 800 °C for 30 min and 900 °C for 10 min. (c) Schematic cross-section of the single material p–i–n photodetector. The mesa size is 32 μm in diameter. (d) Influence of SRV on dark current density of Ge p–i–n photodetector.

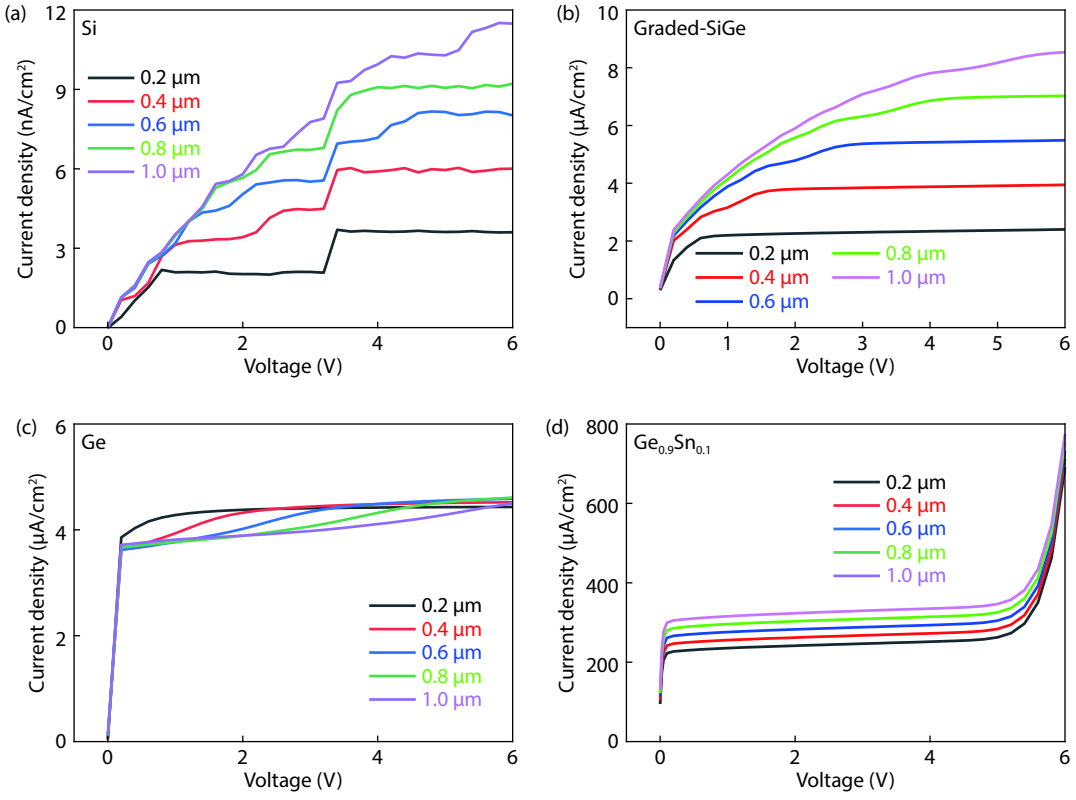

Fig. 4. (Color online) Simulation of J_{dark} of the p–i–n photodetector with single material for (a) Si, (b) graded-SiGe, (c) Ge, and (d) $Ge_{0.9}Sn_{0.1}$.

generally smaller than measured in the experiment. The J_{dark} of graded-SiGe and Ge are of the same order of magnitude. The J_{dark} of the $Ge_{0.9}Sn_{0.1}$ is much larger mainly due to the small bandgap of $Ge_{0.9}Sn_{0.1}$ material, which is two orders of magnitude higher than that in Ge material. This is consistent with former reports[12, 21].

Based on this analysis, to keep the absorption peak of each material at different positions and control the thickness

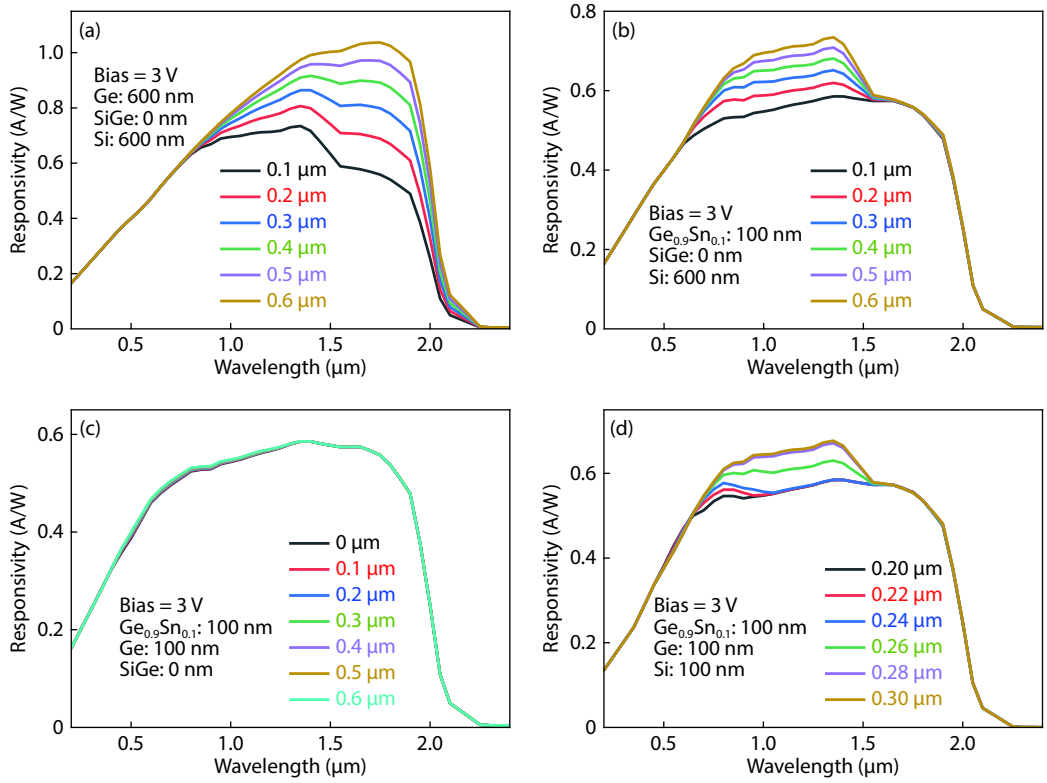

Fig. 5. (Color online) The variation of responsivity under different active region is simulated for (a) $Ge_{0.9}Sn_{0.1}$, (b) Ge, (c) Si, and (d) graded-SiGe.

of the active region within a reasonable range, we superimposed Si, Ge and $Ge_{0.9}Sn_{0.1}$ from top to bottom in the active region. The thickness of each layer in the active region was set to 600 nm. We simulated the spectral response of the device as shown in Fig. 5(a). One can see that the cut-off wavelength is about 2300 nm. To flatten the response, we reduced the thickness of $Ge_{0.9}Sn_{0.1}$ from 600 to 100 nm. The responsivity at 1800 nm is reduced to about 0.57 A/W, it is still an acceptable value. To maximize the range of the flat response, we set the thickness of $Ge_{0.9}Sn_{0.1}$ to 100 nm and reduced the thickness of the Ge layer, as shown in Fig. 5(b). We find that when the thickness of Ge layer is between 100 and 200 nm, it is consistent with the tendency of flat response. Considering the contribution of the Si and graded-SiGeabsorption layers in the Vis optical signal, we set the thickness of Ge layer to 100 nm. It can be observed from Fig. 5(c) that when the thickness of the Si layer is between 0 and 600 nm, there is no significant effect on the spectral response. This happens because that the absorption coefficient of Ge is much larger than that of Si in the Vis range. A thin Si layer in active region cannot improve the responsivity of the photodetector. However, in the process of growth and annealing, i-Si plays an important role as a pure diffusion source and a barrier to resist the diffusion of doped elements from p^+-substrates to the Ge layer. To match the conditions of the experiment, we set the thickness of Si layer to 100 nm. Finally, we simulated the effect of graded-SiGe layer on the spectral response when the thickness is 200 to 300 nm, as shown in Fig. 5(d). To maintain the coefficient characteristics of graded-SiGe, the thickness is controlled in some range. This suggests that when the thickness of the graded-SiGe layer is set to 240 nm, the spectral response is relatively flat. The responsivity of this photodetector is about 0.57 A/W in the range of 700 to 1800 nm.

In the procedure of regulating the thickness of different materials in the active region, when the thickness of the $Ge_{0.9}Sn_{0.1}$ layer is reduced from 600 to 100 nm, the J_{dark} is reduced from 0.22 to 0.17 mA/cm^2, as shown in Fig. 6(a). When the thickness of other materials is changed, the magnitude of the J_{dark} remains the same. This is due to the photodetectors of pure Si, graded-SiGe, and Ge have at least two orders of magnitude lower than that in $Ge_{0.9}Sn_{0.1}$. This structure wraps a thin $Ge_{0.9}Sn_{0.1}$ layer inside the device to reduce the J_{surf} and J_{bulk} of $Ge_{0.9}Sn_{0.1}$. This leads to a reduction in J_{dark}. The spectral response of the designed photodetector and the J_{dark} changes between 0–6 V reverse bias was shown in Fig. 6(b). This indicates that when the reverse bias is below 5 V, the J_{dark} remains stable.

4. Discussion

The graded-SiGe layer is formed by annealing, the thin layer can be obtained easier and more convenient compared with the growth method. The annealing process can also minimize the dislocation in Ge material and introduce a certain tensile strain on the surface of Ge layer. This tensile strain can partially relieve compressive strain caused by large lattice mismatch in the following epitaxial of GeSn layer, thus optimizing the quality of GeSn material[31].

We modulate the thickness of different materials with different absorption peaks to flatten the spectral response. The absorption of Vis optical signal is enhanced by graded-SiGe and the absorption of IR optical signal is expanded by $Ge_{0.9}Sn_{0.1}$, a flat and broad response can be obtained. The thickness of graded-SiGe and Ge layer is controlled in a proper range to avoid the redshift of absorption peak. This can reduce the range and flatness of the flat response. Mean-

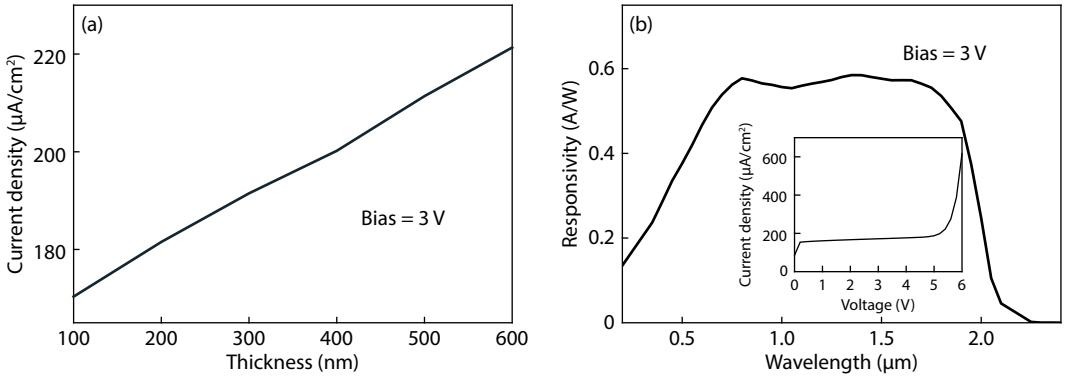

Fig. 6. (a) Magnitude of the J_{dark} at different thickness of $Ge_{0.9}Sn_{0.1}$ layer. (b) The final spectral response of the designed photodetector and the J_{dark} changes between 0–6 V reverse bias.

while, we optimized the structure to effectively mitigate the negative effects of the dead-space effect. The thickness of the active region, especially the $Ge_{0.9}Sn_{0.1}$ material, is greatly reduced, which can be helpful to reduce the dark current density.

Taking into account the actual optical signal incidence, the anti-reflection coating shows the difference in transmission on optical signals of different wavelengths[32]. Therefore, this affects the response characteristic of the photodetector. In the case of introducing the anti-reflection coating to enhance the light incidence efficiency, to obtain a flat response of the device, we can modulate the structure of the active region to compensate for the absorption of the detector in the wavelength range with low transmission of the anti-reflection coating. To enhance the light absorption of the device, in addition to the anti-reflection coating, plasmon, photonic crystal, microlenses, and black silicon can also be combined to increase the transmittance to obtain the expected response characteristic and reduce the impact of the anti-reflection coating on the device[33–36].

5. Conclusions

In summary, a high-performance Si/graded-SiGe/Ge/$Ge_{0.9}Sn_{0.1}$ p–i–n photodetector with flat and broad response is achieved by theoretical study. The p–i–n photodetector consists of entirely group IV materials and reaches a responsivity as high as 0.57 A/W at a range of 700 to 1800 nm. This range covers all of the communication bands. The graded-SiGe layer formed by annealing is beneficial to improve the quality of Ge and $Ge_{0.9}Sn_{0.1}$ layer. The cut-off wavelength of the broadband photodetector is about 2300 nm, the dark-current density is as low as 0.17 mA/cm^2 under a reverse bias of 3 V due to the theoretical optimization. This work shows a prospective method to fabricate broadband p–i–n photodetectors with flat response. This is of significant help to the simplification of subsequent circuits and the improvement of accuracy in the detection system, and has great importance in cost-effective integrated Si photonics.

Acknowledgements

This work was supported by National Basic Research Program of China (No. 2013CB632103), National Natural Science Foundation of China (Nos. 61534005 and 61474081), and Scientific Research Project of Fujian Provincial Department of Education (No. JA15651).

References

[1] Eda G, Fanchini G, Chhowalla M. Large-area ultrathin films of reduced graphene oxide as a transparent and flexible electronic material. Nat Nanotechnol, 2008, 3, 270

[2] Park S, Wang G, Cho B, et al. Flexible molecular-scale electronic devices. Nat Nanotechnol, 2012, 7, 438

[3] de Arquer F P G, Armin A, Meredith P, et al. Solution-processed semiconductors for next-generation photodetectors. Nat Rev Mater, 2017, 2, 16100

[4] Gong X, Tong M, Xia Y, et al. High-detectivity polymer photodetectors with spectral response from 300 nm to 1450 nm. Science, 2009, 325, 1665

[5] Qiao H, Yuan J, Xu Z Q, et al. Broadband photodetectors based on graphene–Bi_2Te_3 heterostructure. ACS Nano, 2015, 9, 1886

[6] Yuan H, Liu X, Afshinmanesh F, et al. Polarization-sensitive broadband photodetector using a black phosphorus vertical p–n junction. Nat Nanotechnol, 2015, 10, 707

[7] Hu W, Cong H, Huang W, et al. Germanium/perovskite heterostructure for high-performance and broadband photodetector from visible to infrared telecommunication band. Light: Sci Appl, 2019, 8, 106

[8] Eckhardt C, Hummer K, Kresse G. Indirect-to-direct gap transition in strained and unstrained Sn_xGe_{1-x} alloys. Phys Rev B, 2014, 89, 165201

[9] Du W, Ghetmiri S A, Conley B R, et al. Competition of optical transitions between direct and indirect bandgaps in $Ge_{1-x}Sn_x$. Appl Phys Lett, 2014, 105, 051104

[10] Gassenq A, Gencarelli F, van Campenhout J, et al. GeSn/Ge heterostructure short-wave infrared photodetectors on silicon. Opt Express, 2012, 20, 27297

[11] Cong H, Xue C L, Zheng J, et al. Silicon based GeSn p–i–n photodetector for SWIR detection. IEEE Photonics J, 2016, 8, 1

[12] Su S J, Cheng B W, Xue C L, et al. GeSn p–i–n photodetector for all telecommunication bands detection. Optics Express, 2011, 19, 6400

[13] Mathews J, Roucka R, Xie J, et al. Extended performance GeSn/Si(100) p–i–n photodetectors for full spectral range telecommunication applications. Appl Phys Lett, 2009, 95, 133506

[14] Kouvetakis J, Menendez J, Chizmeshya A V G. Tin-based group IV semiconductors: New platforms for opto- and microelectronics on silicon. Annu Rev Mater Res, 2006, 36, 497

[15] Ke S Y, Ye Y J, Lin S M, et al. Low-temperature oxide-free silicon and germanium wafer bonding based on a sputtered amorphous Ge. Appl Phys Lett, 2018, 112, 041601

[16] Ke S Y, Ye Y J, Wu J Y, et al. Interface characteristics and electrical transport of Ge/Si heterojunction fabricated by low-temperature wafer bonding. J Phys D, 2018, 51, 265306

[17] Ke S Y, Lin S M, Ye Y J, et al. Bubble evolution mechanism and

stress-induced crystallization in low-temperature silicon wafer bonding based on a thin intermediate amorphous Ge layer. J Phys D, 2017, 50, 405305

[18] Lin Y, Lee K H, Bao S, et al. High-efficiency normal-incidence vertical p–i–n photodetectors on a germanium-on-insulator platform: Publisher's note. Photonics Res, 2018, 6, 46

[19] Ghetmiri S A, Du W, Conley B R, et al. Shortwave-infrared photoluminescence from $Ge_{1-x}Sn_x$ thin films on silicon. J Vac Sci Technol B, 2014, 32, 060601

[20] Tran H, Du W, Ghetmiri S A, et al. Systematic study of $Ge_{1-x}Sn_x$ absorption coefficient and refractive index for the device applications of Si-based optoelectronics. J Appl Phys, 2016, 119, 103106

[21] Masini C, Calace L, Assanto G, et al. High-performance p–i–n Ge on Si photodetectors for the near infrared: From model to demonstration. IEEE Trans Electron Devices, 2001, 48, 1092

[22] Rzaev M, Schäffler F, Vdovin V, et al. Misfit dislocation nucleation and multiplication in fully strained SiGe/Si heterostructures under thermal annealing. Mater Sci Semicond Process, 2005, 8, 137

[23] Humlíček J, Garriga M, Alonso M I, et al. Optical spectra of Si_xGe_{1-x} alloys. J Appl Phys, 1989, 65, 2827

[24] Braunstein R, Moore A R, Herman F. Intrinsic optical absorption in germanium-silicon alloys. Phys Rev, 1958, 109, 695

[25] Choi D, Ge Y S, Harris J S, et al. Low surface roughness and threading dislocation density Ge growth on Si (001). J Cryst Growth, 2008, 310, 4273

[26] Xia G, Hoyt J L, Canonico M. Si–Ge interdiffusion in strained Si/strained SiGe heterostructures and implications for enhanced mobility metal–oxide–semiconductor field-effect transistors. J Appl Phys, 2007, 101, 044901

[27] Gavelle M, Bazizi E M, Scheid E, et al. Study of silicon-germanium interdiffusion from pure germanium deposited layers. Mater Sci Eng B, 2008, 154/155, 110

[28] Luan H, Lim D R, Lee K K, et al. High-quality Ge epilayers on Si with low threading-dislocation densities. Appl Phys Lett, 1999, 75, 2909

[29] del Alamo J, Swirhun S, Swanson R M. Simultaneous measurement of hole lifetime, hole mobility and bandgap narrowing in heavily doped n-type silicon. Int Electron Devices Meet, 1985, 290

[30] Kulin S S, Kurtz A D. Effect of dislocations on minority carrier lifetime in germanium. Acta Metall, 1954, 2, 354

[31] Zhao Y, Wang N, Yu K, et al. High performance silicon-based GeSn p–i–n photodetectors for short-wave infrared application. Chin Phys B, 2019, 28, 128501

[32] Kasai I, Hettich H L, Lawrence S L, et al. Wideband anti-reflection coating for indium antimonide photodetector device. European Patent, EP0585055, 1997

[33] Chang C, Sharma Y D, Kim Y, et al. A surface plasmon enhanced infrared photodetector based on InAs quantum dots. Nano Lett, 2010, 10, 1704

[34] Yang J K, Seo M K, Hwang I K, et al. Polarization-selective resonant photonic crystal photodetector. Appl Phys Lett, 2008, 93, 211103

[35] Zhu T F, Liu Z C, Liu Z C, et al. Fabrication of monolithic diamond photodetector with microlenses. Opt Express, 2017, 25, 31586

[36] Zhong H, Guo A R, Guo G H, et al. The enhanced light absorptance and device application of nanostructured black silicon fabricated by metal-assisted chemical etching. Nanoscale Res Lett, 2016, 11, 1